J Supercond Nov Magn (2014) 27:2779–2786
DOI 10.1007/s10948-014-2703-0

ORIGINAL PAPER

Investigation of Magnetic Entropy Change and Griffiths-like Phase in $La_{0.65}Ca_{0.35}MnO_3$ Nanocrystalline

Lisha Xu · Zhiyue Chen · Xiyuan Zhang · Yangguang Shi · Yan Zhu · Daning Shi · Lei Zhang · Li Pi · Yuheng Zhang · Jiyu Fan

Received: 21 July 2014 / Accepted: 12 August 2014 / Published online: 27 August 2014

Abstract In this paper, we reported a detailed study of magnetic properties and magnetic entropy change of $La_{0.65}Ca_{0.35}MnO_3$ nanocrystalline, which was prepared by using the sol–gel method. The structural analysis shows that the nanocrystalline sample crystalizes in orthorhombic perovskite structure and the average size is about 30 nm. Based on the measurements of magnetization, a larger effective magnetic moment was obtained and an obvious deviation of the inverse magnetic susceptibility was observed, indicating the presence of Griffiths-like phase in paramagnetic region. Around the temperature of paramagnetic–ferromagnetic phase transition, the magnetocaloric effect (as represented by the magnetic entropy change) was determined from isothermal magnetization and calculated with Maxwell relation. Compared with bulk polycrystalline, the obtained magnetic entropy change in nanocrystalline is small. This result clearly reveals that the decrease of the sample's size to nanoscale is detrimental for the increase of magnetocaloric effect of magnetic materials. Besides the particle size and surface effect, the paramagnetic–ferromagnetic phase transition driven from first to second order should be a main reason for the small magnetocaloric effect in $La_{0.65}Ca_{0.35}MnO_3$ nanocrystalline.

L. Xu · Z. Chen · X. Zhang · Y. Shi · Y. Zhu · D. Shi · J. Fan (✉)
Department of Applied Physics, Nanjing University of Aeronautics and Astronautics, Nanjing 210016, China
e-mail: jiyufan@nuaa.edu.cn

L. Zhang · L. Pi · Y. Zhang
High Magnetic Field Laboratory, Chinese Academy of Sciences, Hefei 230031, China

Keywords Manganite · Magnetocaloric effect · Nanocrystalline · Phase transitions

1 Introduction

Magnetocaloric effect (MCE) is described as the isothermal change of entropy or the adiabatic change of temperature induced by application and removal of magnetic field, which has a great promise for domestic and industrial use due to the advantages such as high-power efficiency, low-energy consuming, and environmental friendliness, compared to conventional vapor-compression refrigeration [1–4]. The rare earth metal gadolinium (Gd) was firstly considered as the most conspicuous material which exhibits a large MCE near room temperature ($|\Delta S_m|$ = 10.2 J/kg K at Δ H =5.0 T, T_C = 294 K) [5]. However, the mass production seems to be impossible due to its expensive cost price. Therefore, the pursuit of a new working substance for magnetic refrigerator with a cheap price and large MCE becomes a main research topic. At present, besides some possible candidates, such as $Gd_5(Si_{1-x}Ge_x)_4$ [6, 7], $MnAs_{1-x}Sb_x$ [8], $MnFeP_{1-x}As_x$ [9] and $Tb_{1-x}Gd_xAl_2$ [10], the hole-doped manganites should be one of the most promising materials since its Curie temperature and magnetic phase transition are strongly doping dependent and the magnetic refrigeration can be realized at various temperatures [11].

The perovskite manganites with the form $A_{1-x}B_xMnO_3$ (A=rare earth element, B=divalent alkaline earth element) have been extensively investigated in the last years due to their unique physical properties, stemming from the close interaction of spin, charge, orbital, and lattice degree of freedom [12–15]. The prototypal spin–charge–lattice-coupled $LaMnO_3$ is an antiferromangnetic and insulating

system [16, 17]. The introduction of holes (Mn^{4+}) into the Mn^{3+} e_g orbital generates the ferromagnetic double exchange interactions which couples the magnetic system with metallic conductivity. Therefore, with the decrease of temperature, the hole-doping manganites $A_{1-x}B_xMnO_3$ generally exhibit a paramagnetic–ferromagnetic (PM-FM) and insulator-metallic (IM) phase transition. Up to present, large MCE has been continually reported in hole-doping manganites [18–22].

As we know, for bulk magnetic materials, their magnetic properties are size and shape dependent when the size is reduced to nanometer scale. Therefore, the MCE is inevitably tuned by the reduction of particle size. The main reason is that the size reduction influences the magnetic order and changes the coupling between spin and lattice subsystem in the doped manganites. Sarkar et al. [23] and Amirzadeh et al. [24] reported that the grain size influenced the magnetostructural phase transition and magnetic homogeneity in $La_{0.65}Ca_{0.35}MnO_3$ (LCMO). Recently, Lampen et al. [25] found the reduced dimensionality tended to decrease the saturation magnetization and broaden paramagnetic–ferromagnetic phase transition in the optimal doping manganite $La_{0.7}Ca_{0.3}MnO_3$. In this paper, we synthesize the nanocrystalline sample $La_{0.65}Ca_{0.35}MnO_3$ (LCMO), and study its magnetism and MCE by the measurement of temperature dependence magnetization and isothermal magnetization. Consistent with the previous observation, the nanocrystalline process weakens the sharp PM-FM phase transition in the prototype bulk sample. As a result, its maximum magnetic entropy change has been distinctly decreased. The intrinsic reason is that the reduced size induces more spin disorder which decreases magnetic coupling among domains and drives the magnetic phase transition from first order to second order in the samples.

2 Experiment

The LCMO nanocrystalline sample was prepared by the sol–gel process with high-purity $La_{0.65}Ca_{0.35}MnO_3$ and $MnCO_3$. They were first converted into nitrates by adding nitric acid with a molar ratio of La/Ca/Mn = 13:7:20. After stoichiometric mixing of the precursor metal nitrate solutions, citric acid was added as a polymerizing agent and the gel was obtained after gradual evaporation of the solvent at 75 °C for 10 h. The gel was dried at 100 °C for 24 h and then preheated to form a black porous powder at 400 °C for 6 h to remove the remaining organic and decompose the nitrates of the gel. Finally, the power was annealed at 800 °C for 4 h. Phase purity and crystal structures were identified by x-ray diffraction (XRD) using Cu Kα radiation at room temperature. The microstructure was identified by field-emission scanning electron microscopy (FESEM). The magnetic measurements were carried out using a commercial superconducting quantum interference device magnetic property measurement system.(SQUID VSM-Quantum Design, Inc.)

3 Results and Discussion

Figure 1 shows the XRD patterns of LCMO nanocrystalline, which suggests that the sample are a single phase with the orthorhombic (Pnma) structure. The XRD peaks are broad with large full width at half maximum (FWHM), indicating the formation of LCMO nanocrystals. As shown in the insert of Fig. 1, the size of LCMO particles is homogeneous and the average diameter is about 30 nm estimated through FESEM. Moreover, the average particle size d can be calculated with the Scherrer's formula

$$d = \frac{k\lambda}{\beta\cos\theta} \tag{1}$$

where $k = 0.89$ is the particle shape factor, considering the spherical shape in the present nanocrystalline sample, $\lambda = 0.15406$ nm is the wavelength of Cu Kα radiation, β and θ are the full width at half maximum of XRD (110) peak and the diffraction angle of this peak, respectively. The calculated average particle size is about 25.6 nm, basically consistent with the observation from the FESEM.

Figure 2 shows the temperature dependence of magnetization (*M-T*) of LCMO measured in the magnetic field of 100 Oe (left hand axis), which exhibits a PM-FM transition. The PM-FM transition temperatures (T_C) is about 235 K obtained from the peak of *dM/dT* curves (not shown here). The right axis of Fig. 2 presents the inverse magnetic susceptibility as a function of temperature and the fitting results according to the Curie-Weiss Law (dashed lines) and Griffiths model (solid lines), respectively. The Curie-Weiss law is presented as $\chi = C/(T - \theta_P)$, where C is the Curie constant and θ_P is the Weiss temperature. As shown in Fig. 2, obviously, the Curie-Weiss law is not satisfied with the experimental curves in the whole PM range. The deviation of the inverse susceptibility χ^{-1} from the high-temperature straight line implies the onset of the FM interaction between magnetic moments above T_C. The phenomenon allows us to argue the possible appearance of Griffiths singularity which is characterized by a susceptibility exponent between less than unity; that is, $\chi(T)^{-1} \propto (T - T_G)^{1-\lambda}$, where T_G is the temperature for the Griffiths phase formation [26]. The solid line in Fig. 2 is the fitting result and the corresponding fitting parameters λ and T_G are 0.375 and 270 K, respectively. The Griffiths phase is some FM clusters formed in the PM phase matrix, which commonly is observed in doped manganites. [27, 28] The observed Griffiths-like phase in this sample is related to the local FM fluctuations, which might

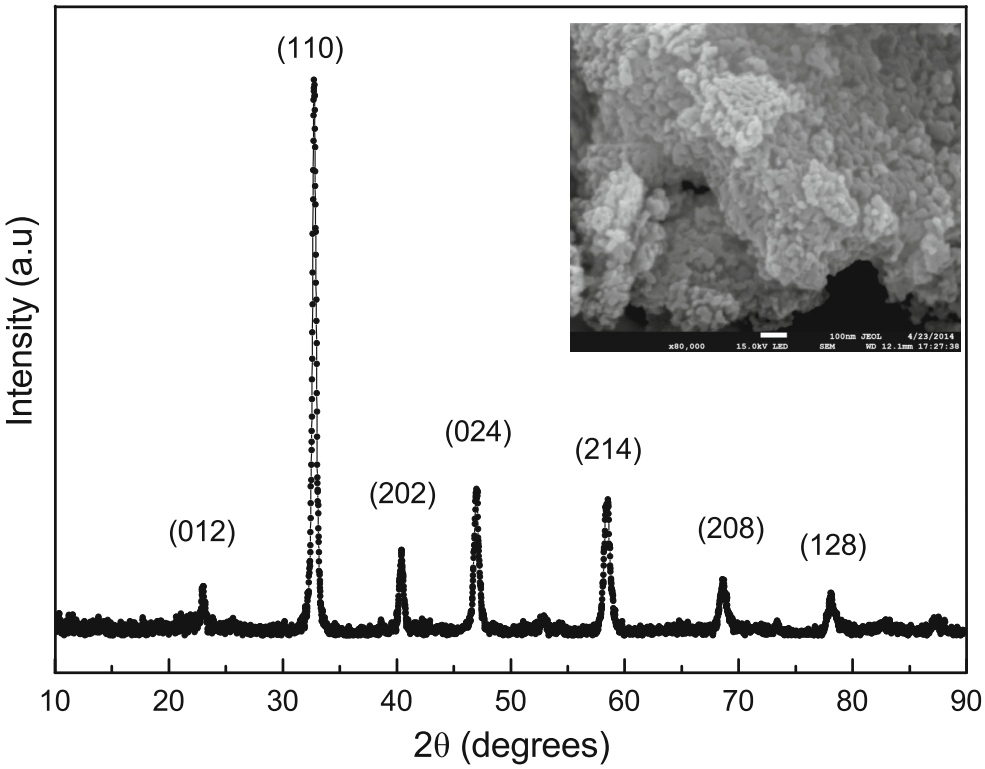

Fig. 1 (Color online) The x-ray diffraction patterns of $La_{0.65}Ca_{0.35}MnO_3$. *Insert* SEM micrographs of $La_{0.65}Ca_{0.35}MnO_3$

be ascribed to the random spatial variation in magnetic exchange interactions. The local FM interactions above T_C can be further evidenced from the effective magnetic moment (μ_{eff}). It can be deduced from the inverse magnetic susceptibility with $\mu_{\text{eff}} = 2.82\sqrt{C}$. The obtained μ_{eff} value is 5.674 μ_B. which is larger than the calculated value using the spin-only moment of the free Mn ions in LCMO (3.87 μ_B for Mn^{+4} and 4.90 μ_B for Mn^{3+}). Therefore, the larger effective magnetic moment implies the possible existence of FM coupling in PM region.

In order to further testify the existence of Griffiths phase, the isothermal magnetization (M-H) are measured at two selected temperatures. One is above T_G and the other is below T_G. Panels a and b of Fig. 3 shows the corresponding magnetic hysteresis loops at $T = 265$ K and $T = 275$ K, respectively. It is clear that the magnetization are

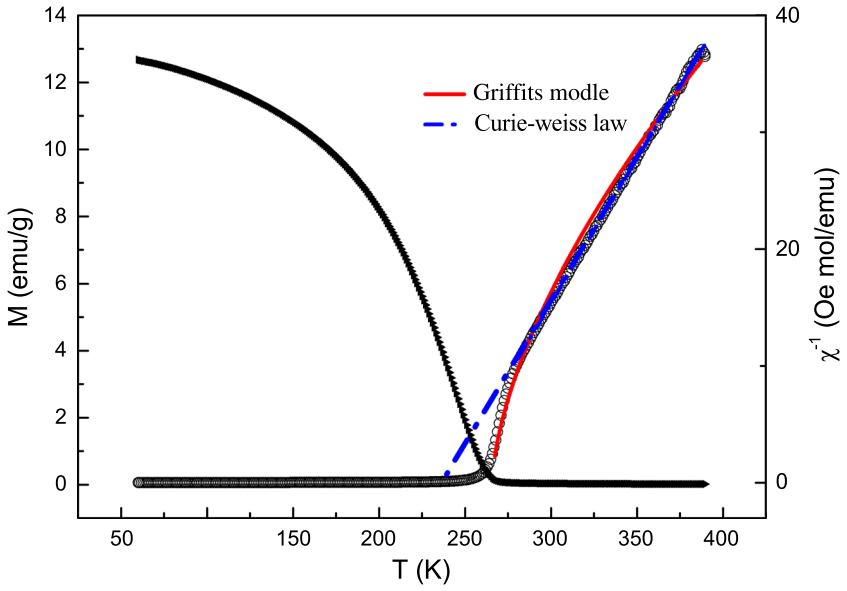

Fig. 2 (Color online) *Left axes* Temperature dependence of magnetization measured at $H = 100$ Oe. *Right axes* Inverse susceptibility as a function of temperature for $La_{0.65}Ca_{0.35}MnO_3$. The *dash lines* represent the fitting data according to the Curie-Weiss law and the *solid line* is the fitting result following the Griffiths model

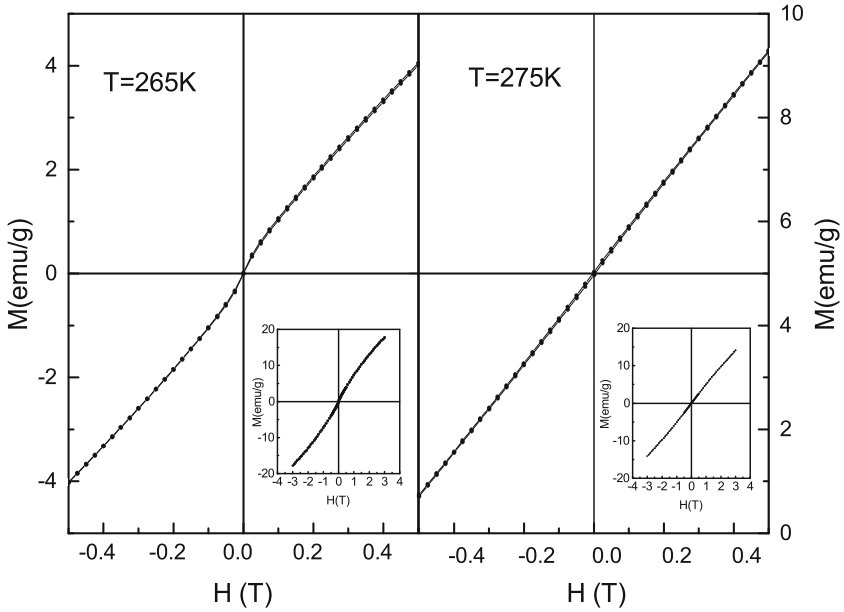

Fig. 3 (Color online) Magnetic hysteresis loops of $La_{0.65}Ca_{0.35}MnO_3$ at 265 K **(a)** and 275 K **(b)**. Inset shows the isothermal magnetizations with the whole sweep magnetic field from 3 to -3 T

unsaturation and there are no magnetization hysteresis to be measured. One typical PM behavior can be observed for both temperatures. However, a slight difference between them is easily found in the low magnetic field region. At $T = 275$ K, higher than T_G, its magnetic hysteresis loop keeps a completely linear variation with the magnetic field up to 3.0 T. On the contrary, at $T = 265$ K, lower than T_G, its magnetic hysteresis loop is not an absolute linear curve but shows a perceivable inflection, indicating the existence of FM character. Similar to the present results, the Griffiths phase has been also observed in $La_{0.65}Ca_{0.35}MnO_3$ nanoparticles by Lu et al. [29] where they found the Griffiths phase disappeared as the nanoparticle size increases above 51 nm. Generally, quenched disorder is prerequisite for formation of the Griffiths phase. Even though perovskite manganites are generally thought to be an intrinsically disorder system due to the ionic random distribution on A-site sublattice. However, the Griffiths phase has never been reported in bulk polycrystalline LCMO counterpart. Moreover, nanocrystalline derived by sol–gel method has a better ionic homogeneity than polycrystalline obtained by solid-state reaction method. Therefore, the reason for the formation of the Griffiths phase is different from the general situation. We proposed that as the spatial size was decreased to nanoscale, the increasing surface spin could weaken the inner magnetic coupling, similar to the doping method to break the long-range FM interaction. Thus, the localized FM state can appear earlier than that in buck sample and the Griffiths phase occurs in the nanomaterials above its Curie temperature.

Apart form the above analysis on the magnetization, we will focus on the investigation of MCE in $La_{0.65}Ca_{0.35}MnO_3$ nanocrystalline in the following section.

In order to evaluate the magnetic entropy change in the system, as shown in Fig. 4, a series of isothermal magnetization curves from 110 to 300 K were measured. The isothermal magnetic entropy change ΔS_M as a function of temperature can be calculated with Maxwell relation as follows:

$$\Delta S(T, H) = S_M(T, H) - S_M(T, 0) = \int_0^H \left(\frac{\partial M(T, H)}{\partial T}\right) dT \quad (2)$$

In practice, the magnetic entropy change $|\Delta S_M|$ can be evaluated from the isothermal magnetization measured with small temperature intervals, where $\Delta S_M(T, H)$ can be approximated as

$$|\Delta S_M| = \sum \frac{M_i - M_{i+1}}{T_{i+1} - T_i} \Delta H_i \quad (3)$$

where M_i and M_{i+1} are the experimental data of the magnetization at T_i and T_{i+1}, respectively, under a magnetic field H_i. By using (3), the magnetic entropy change vs temperature under different magnetic fields are presented in Fig. 5a, and the obtained maximum magnetic entropy change are 0.25, 0.55, 0.80, 1.06, 1.34, 1.56 J/kg for 0.5, 1.0, 1.5, 2.0, 2.5, 3.0 T, respectively. The value of magnetic entropy change increases with the increase of magnetic field. From Fig. 5a, one can find that ΔS_M distributes over a wide temperature range, and the maximum S_M is much smaller than that of bulk sample. Here, the small magnetic entropy change obtained in nanocrystalline clearly indicates that the size reduced to nanoscale is detrimental for the increase of MCE of magnetic material.

Beside magnetic entropy change, the value of cooling power is also another important parameter for actual application in magnetic refrigeration. The cooling power is

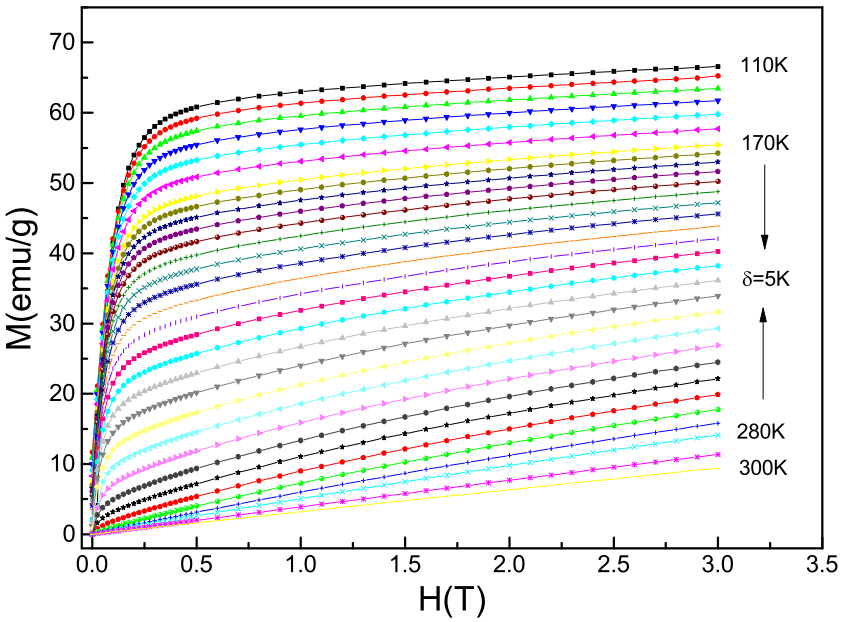

Fig. 4 (Color online) Isothermal magnetization measured at different temperatures for $La_{0.65}Ca_{0.35}MnO_3$ nanocrystalline

characterized with refrigerant capacity power (RCP). The large RCP indicates more heat to be transferred from the cold end to the hot end of the refrigerator in one thermodynamic cycle. RCP is generally calculated by integrating the $(\Delta S_M - T)$ curves over the full width at half maximum with the relation:

$$RCP = -\Delta S_{\mathrm{Mmax}} \delta T_{\mathrm{FWHM}} \tag{4}$$

Where δT_{FWHM} is the FWHM of the magnetic entropy change curve. As shown in Fig. 5b, the obtained RCP values increase with the applied magnetic field indicating that RCP is strong field dependent. In fact, RCP depends on magnetic field H as RCP $= aH^b$ [30]. By using it, as shown in Fig. 5b, the fitting value of b is ∼1.06. On the other hand, from the critical analysis point of view, the value of b is satisfied with the following relationship: $b = 1 + \frac{1}{\delta}$, where δ is one of critical exponents and associated with the critical magnetization isotherm at $T_C (M_{T=T_C} \propto H^{1/\delta})$. The value of δ can be obtained by fitting $M(H)$ curves. As shown in Fig. 5c, the fitting value of δ is 3.46. Therefore, the value of b is 1.29, which approximates to the experimental results.

In order to study the origin of MCE, a simple theoretical model based on the magnetoelastic couplings and electron interaction was introduced in manganites. Based on the Landau theory, the Gibbs free energy can be expressed in terms

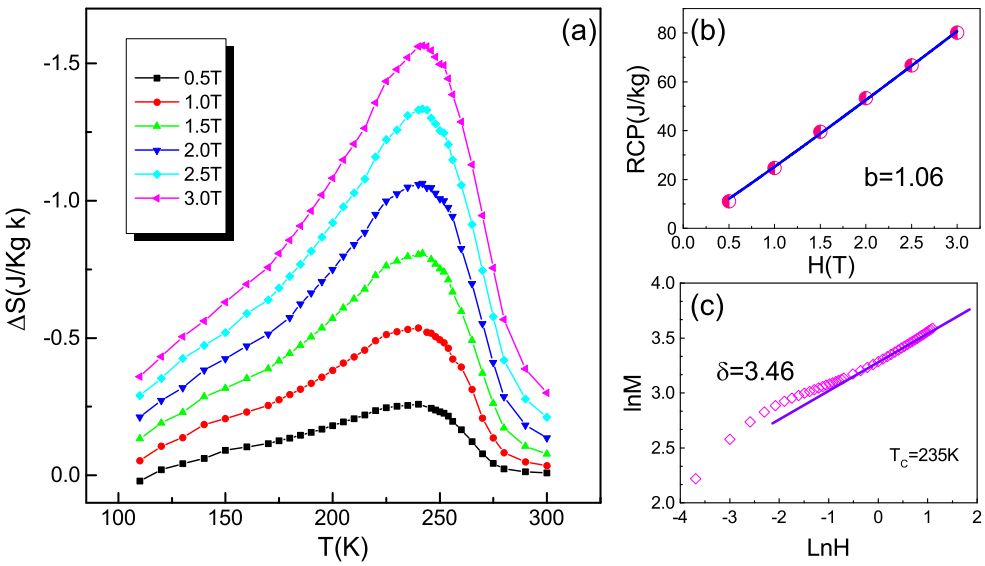

Fig. 5 (Color online) **a** Magnetic entropy change ΔS plotted as a function of temperature at different applied fields. **b** Refrigerant capacity as a function of applied magnetic field, the *solid line* is the fitting results following RCP = aH^b. **c** The isothermal magnetization at T_C is plotted in log–log scale, and the *solid line* is the linear fit following M∝ $H^{1/\delta}$

of the order parameter M in the following form neglecting higher order parts:

$$G(T, M) = G_0 + \frac{1}{2}AM^2 + \frac{1}{4}BM^2 - MH \quad (5)$$

Where the coefficients of A and B are temperature-dependent parameters. For the condition of equilibrium, i.e., energy minimization, $\frac{\partial G}{\partial T}$=0, the magnetic equation of state is obtained as

$$\frac{H}{M} = A + BM^2 \quad (6)$$

Thus, the relationship of M^2 vs (H/M) should be shown as a linear behavior around T_C. According to the criterion proposed by Banerjee [31], the order of magnetic transition can be determined from the slope of a straight line. The positive slope corresponds to the second-order transition while the negative slope corresponds to the first-order transition. Figure 6 is an Arrott plot of M^2 vs (H/M). Clearly, in the present case the positive slope of M^2 vs (H/M) curves indicates that the phase transition is a second-order PM-FM phase transition. The parameters A and B are also deduced from the linear fitting of the Arrott plot (shown as insert of Fig. 6). One can find that parameter A varies from negative to positive values with increasing temperature. As parameter A equals to zero, the corresponding temperature is just T_C. Parameter B is correlated with the elastic and the magnetoelastic terms for magnetic entropy change in manganites [35, 36]. However, different from the variation of B in bulk polycrystalline where the B value always keeps decreasing when the temperature approaches to T_C from high temperature [37], here, it first increases and then decreases. Therefore, in the nanocrystalline sample, other factors including the particle size and surface effect also impact on the value of parameter B.

Obviously, based on the second-order PM-FM phase transition in the current LCMO, we study its magnetism and MCE. However, Franco et al. thought that it is not completely accurate for judging the second-order phase transition only from the Arrott plot [32, 33]. Recently, they proposed a phenomenological model to demarcate the order of PM-FM phase transition. Franco et al. [34] According to the method, the rescaled ΔS_M vs T curves under different magnetic fields collapse into a single curve only for the second-order materials. Therefore, the order of phase transition in the present system should be further clarified by utilizing this method. First, two points are selected from each ΔS_M vs. T curves. One(T_{r1}) is below T_{peak} and the other (T_{r2}) is above T_{peak}. Both of them should satisfy the relation $\Delta S_M(T_{r1}) = \Delta S_M(T_{r2}) = k\Delta S_M^{\text{peak}}(T_{\text{peak}})$, where ΔS_M^{peak} is the maximum value of the selected ΔS_M vs T curves and k is the relative value of the entropy changes at two reference temperatures T_{r1} and T_{r2}. Generally, the selection of k value is arbitrary but k value is always between 0 and 1. Here, we choose the $k = 0.7$ to construct the "universal master curve." Two reference temperatures are used here and the temperature axis is rescaled as:

$$\theta = \begin{cases} \theta_- = (T_{\text{peak}} - T)/(T_{r1} - T_{\text{peak}}), & T < T_{\text{peak}} \\ \theta_+ = (T - T_{\text{peak}})/(T_{r2} - T_{\text{peak}}), & T > T_{\text{peak}} \end{cases} \quad (7)$$

As shown in Fig. 7, all the ΔS_M vs. T curves collapse into a single curve. Therefore, the PM-FM phase transition in LCMO was confirmed to be second order. At present, there are different methods to drive the magnetic phase transition from first to second order. The applications of magnetic field and pressure are the most frequent means.

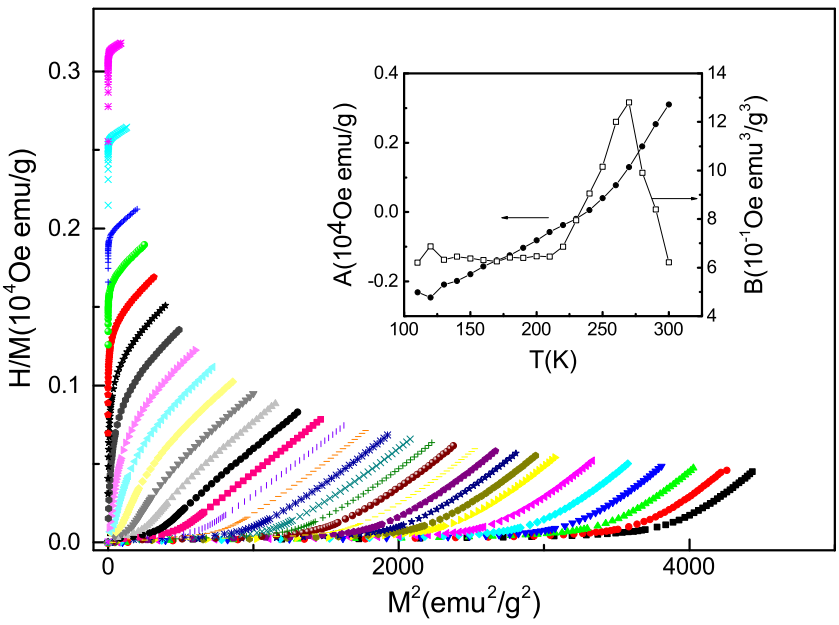

Fig. 6 (Color online) Isotherms of H/M vs M^2 at different temperatures close to the Curie temperature ($T_C = 235$ K). *Inset* temperature dependence of parameters A *(left hand)* and B *(right hand)*

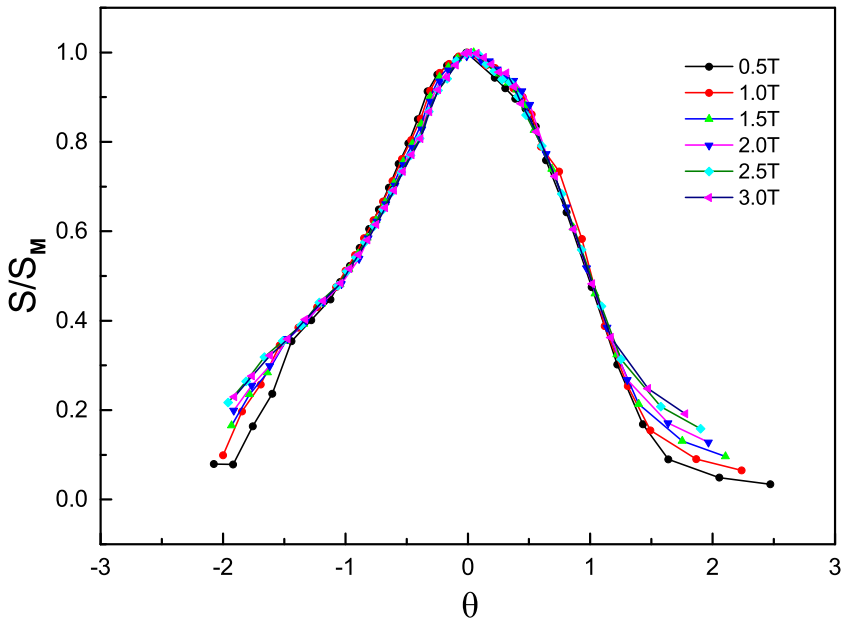

Fig. 7 (Color online) Normalized magnetic entropy change dependence of the rescaled temperatures

For the bulk polycrystalline LCMO, it's PM-FM phase transition belongs to the first order. As it becomes the present nanocrystalline, the PM-FM phase transition changes to second order. For the first order materials, it's magnetic entropy change is generally very large. On the contrary, the magnetic entropy change of second order materials is very small. Therefore, the main reason for a relatively small magnetic entropy change to be observed in LCMO nanocrystalline is due to the PM-FM phase transition changed from first order to second order. Other possible reasons are due to the increasing surface spin in nanocrystalline which weakens the magnetic coupling among domains. As a result, the PM-FM phase transition process is broadened and it brings a small $\frac{\partial(M)}{\partial(T)}$ in formula (2). Moreover, the particle size and particle boundaries are also considered to affect magnetic entropy change in nanocrystalline materials.

4 Conclusion

In summary, we have studied magnetocaloric effect and Griffiths-like phase of LCMO nanocrystalline. The experimental results indicate that when the grain size is reduced to 30 nm the Griffiths-like phase occurs. From the calculation of magnetic entropy change, one can find that the obtained magnetocaloric effect of LCMO nanocrystalline is very small, indicating the nanocrystallization decreases the magnetocaloric effect in magnetic materials. Based on the scaling analysis, the present PM-FM phase transition belongs to the second order, which is the main reason for the small magnetic entropy change obtained in the present LCMO nanocrystalline.

Acknowledgments This work was supported by the National Nature Science Foundation of China (grant nos. 11004196, 11204131, 11204270, and U1332140).

References

1. Zhang, X.X., Taiada, J., Xin, Y., Sunm, G.F., Wong, K.W., Bohigas, X.: Appl. Phys. Lett. **69**, 3596 (1996)
2. Gordon, J.E., Fisher, R.A., Jia, Y.X., Phillips, N.E., Reklis, S.F., Wright, D.A., Zettl, A.: J. Magn. Magn. Mater. **177**, 856 (1998)
3. Bohigas, X., Tejada, J., Del Barco, E., Zhang, X.X., Sales, M.: Appl. Phys. Lett. **73**, 390 (1998)
4. Bohigas, X., Del Barco, E., Sales, M., Tejada, J.: J. Magn. Magn. Mater. **196**, 455 (1999)
5. Dankov, S.Y., Tishin, A.M., Pecharsky, V.K., Gschneidner Jr, K.A.: Phys. Rev. B **57**, 3478 (1998)
6. Pecharsky, V.K., Gschneidner, K.A.: Phys. Rev. Lett. **78**, 4494 (1997)
7. Pecharsky, V.K., Gschneidner, K.A.: Appl. Phys. Lett. **70**, 3299 (1997)
8. Wada, H., Tanabe, Y.: Appl. Phys. Lett. **79**, 3302 (2001)
9. Tegus, Q., Bruck, E., Buschow, K.H., de Boer, F.R.: Nature **415**, 150 (2002)
10. Wang, F.W., Zhang, X.X., Hu, F.X.: Appl. Phys. Lett. **77**, 1360 (2000)
11. Phan, M.H., Yu, S.C., Magn, J.: Magn. Mater. **308**, 325 (2007)
12. von Helmolt, R., Wecker, J., Holzapfel, B., Schultz, L., Samwer, K.: Phys. Rev. Lett. **71**, 2331 (1993)
13. Jin, S., Tiefel, T.H., McCormack, M., Fastnacht, R.A., Ramesh, R., Chen, L.H.: Science **264**, 413 (1994)
14. Rao, C.N.R., Cheetham, A.K.: Science **276**, 911 (1999)
15. Mori, S., Chen, C.H., Cheong, S.-W.: Phys. Rev. Lett. **81**, 3972 (1998)
16. DeGennes, E.P.G.: Phys. Rev. **118**, 141 (1960)
17. Goodenough, J.B.: Phys. Rev. **171**, 466 (1968)
18. Phan, M.H., Peng, H.X., Yu, S.C.: J. Appl. Phys. **97**, 10M306 (2005)

19. Sarkar, T., Ghosh, B., Raychaudhuri, A.K., Szewczyk, T.C., Gutowska, M., Dabrowski, B., Plackowski, T., Danilova, N.P., Gaidukov, Y.P.: Phys. Rev. B **71**, 224432 (2005)
20. Rebello, A., Naik, V.B., Mahendiran, R.: J. Appl. Phys. **110**, 013906 (2011)
21. Rubi, K., Kumar, P., Maheswar Repaka, D., Chen, R.uofan., Shen, J.ian.-W.ang., Mahendiran, R.: Appl. Phys. Lett. **104**, 032407 (2014)
22. Moya, X., Hueso, L.E., Maccherozzi, F., Tovstolytkin, A.I., Podyalovskii, D.I., Ducati, C., Phillips, L.C., Ghidini, M., Hovorka, O., Berger, A., Vickers, M.E., Defay, E., Dhesi, S.S., Mathur, N.D.: Nat. Mater. **12**, 52 (2012)
23. Sarkar, T., Ghosh, B., Raychaudhuri, A.K., Chatterji, T.: Phys. Rev. B **77**, 235112 (2008)
24. Amirzadeh, P., Ahmadvand, H., Kameli, P., Aslibeiki, B., Salamati, H., Gamzatov, A.G., Aliev, A.M., Kamilov, I.K.: J. Appl. Phys. **113**, 123904 (2013)
25. Lampen, P., Bingham, N.S., Phan, M.H., Kim, H., Osofsky, M., Piqué, A., Phan, T.L., Yu, S.C., Srikanth, H.: Appl. Phys. Lett. **102**, 062414 (2013)
26. Salamon, M.B., Lin, P., Chun, S.H.: Phys. Rev. Lett. **88**, 197203 (2002)
27. Fan, J.iyu., Li, P.i., He, Y.an., Ling, L.angsheng., Dai, J.ixia., Zhang, Y.uheng.: J. Appl. Phys. **101**, 123910 (2007)
28. Deisenhofer, J., Braak, D., Krug von Nidda, H.A., Hemberger, J., Eremina, R.M., Ivanshin, V.A., Balbashov, A.M., Jug, G., Loidl, A., Kimura, T., Tokura, Y.: Phys. Rev. Lett. **95**, 257202 (2005)
29. Lu, W.J., Luo, X., Hao, C.Y., Song, W.H., Sun, Y.P.: J. Appl. Phys **104**, 113908 (2008)
30. Franco, V., Conde, A.: Int. J. Refrig. **33**, 465 (2010)
31. Banerjee, S.K.: Phys. Lett. **12**, 16 (1964)
32. Bonilla, C.M., Herrero-Albillos, J., Bartolome, F., Garcia, L.M., Parra-Borderias, M., Franco, V.: Phys. Rev. B **81**, 224424 (2010)
33. Franco, V., Blazquez, J.S., Conde, A.: Appl. Phys. Lett. **89**, 222512 (2006)
34. Franco, V., Conde, A., Romero-Enrique, J.M., Blazquez, J.S.: J. Phys. Condens. Matter. **20**, 285207 (2008)
35. Amaral, V.A., Amaral, J.S.: J. Magn. Magn. Mater. **272**, 2104 (2004)
36. Amaral, J.S., Reis, M.S., Amaral, V.A., Mendonca, T.M., Araúji, J.P., Sá, M.A., Tvares, P.B., Vieira, J.M.: J. Magn. Magn. Mater. **290**, 686 (2005)
37. Fan, J., Pi, L., Zhang, L., Tong, W., Ling, L., Hong, B., Shi, Y., Zhang, W., Lu, D., Zhang, Y.: Physica B **406**, 2289 (2011)